# Self-assembled type I collagen-apatite fibers with varying mineralization extent and luminescent terbium promote osteogenic differentiation of mesenchymal stem cells

*Ismael Romero-Castillo, Elena López-Ruiz, Jorge Fernando Fernández-Sánchez, Juan Antonio Marchal and Jaime Gómez-Morales**

I. Romero-Castillo, Dr. Jaime Gómez-Morales
Laboratorio de Estudios Cristalográficos, IACT–CSIC–UGR. Avda. Las Palmeras, nº 4. E–18100 Armilla (Granada), Spain.
Corresponding autor. E-mail: jaime@lec.csic.es

Dr. E. López-Ruiz, Prof. J.A. Marchal
Instituto de Investigación Biosanitaria ibs. Granada, University of Granada, E-18014 Granada, Spain.
Biopathology and Regenerative Medicine Institute (IBIMER), Centre for Biomedical Research, University of Granada, E-18100 Granada, Spain.
Excellence Research Unit "Modelling Nature" (MNat), University of Granada, Spain.

Dr. E. López-Ruiz.
Dept. Health Science, Faculty of Experimental Science, University of Jaén, 23071 Jaén, Spain.

Prof. J. F. Fernández-Sánchez
Dept. Analytical Chemistry, Faculty of Sciences, University of Granada, Avda. Fuentenueva s/n, 18071 Granada, Spain.

Keywords: type I-collagen, self-assembly, apatite mineralization, terbium; hMSCs cell viability; hMSCs osteogenic differentiation.

This work explores in depth the simultaneous self-assembly and mineralization of type I collagen by a base-acid neutralization technique to prepare biomimetic collagen-apatite fibrils with varying mineralization extent and doped with luminescent bactericidal $Tb^{3+}$ ions. Two variants of the method were tested: base-acid titration, a solution of $Ca(OH)_2$ was added dropwise to a stirred solution containing type I collagen dispersed in $H_3PO_4$ ; and direct mixing, the $Ca(OH)_2$ solution was added by fast dripping onto the acidic solution. Only the direct mixing variant yielded an effective control of calcium phosphate polymorphism. Luminescence spectroscopy revealed the long luminescence lifetime and high relative luminescence intensity of the $Tb^{3+}$-doped materials, while two-photon confocal fluorescence microscopy showed the

characteristic green fluorescence light when using excitation wavelength of 458 nm, which is not harmful to bone tissue. Cytotoxicity/viability tests revealed that direct mixing samples showed higher cell proliferation than titration samples. Additionally, osteogenic differentiation essays showed that all mineralized fibrils promoted the osteogenic differentiation, but the effect was more pronounced when using samples prepared by direct mixing, and more notably when using the $Tb^{3+}$-doped mineralized fibrils. Based on these findings we conclude the new nanocomposite is an ideal candidate for bone regenerative therapy.

## 1. Introduction

Type-I collagen (Col) is the most abundant structural protein in mammals. It can be found in tendon and epithelial tissues, as well as in bone and teeth, where plays a structural role as an extracellular protein, and determine their mechanical and elastic behaviour. [1,2]

Bone is a mineralized tissue with particular hierarchical architecture, mechanical properties and remodeling capabilities.[2] The basic building unit of the intimate structure of the bone is a self–assembled collagen fibril, mainly type I collagen, mineralized with apatite nanocrystals at both intrafibrillar and interfibrillar zones.[3–6] Type I collagen is a trimeric molecule that consist of two α1 and one α2 peptide chains, formed by a repetitive sequence of glycine–X–Y, with X and Y being normally proline and hydroxyproline residues. Under physiological conditions the collagen molecules self–assemble into triple helical structures forming the so–called tropocollagen. The interaction between tropocollagen units leads to the formation of fibrillar structures with a regular array of gaps and overlap spaces, observed in transmission electron microscopy (TEM) as a periodic banding pattern of 67 nm (D-spacing).[3–6] The mineral component is a poorly crystalline, non-stoichiometric $Ca^{2+}$– and OH–deficient apatite -the stoichiometric hydroxyapatite (HA) is $Ca_{10}(PO_4)_6(OH)_2$-, coated with citrate and doped with 4–6 wt % of carbonate, 0.9 wt% Na, 0.5 wt% Mg and others minor elements.[7,8]

Bone has long fascinated scientists and material engineers, who have devoted big efforts to fabricate biomaterials inspired in it. Because of its structural and chemical similarity with the basic building block of bone,[2] synthetic biomimetic collagen/apatite nanocomposite is one of most suitable system for bone replacement or regenerative therapy. The combination of collagen with calcium phosphate (CaP) is necessary to become osteoinductive and also to accelerate osteogenesis.[1] The mineral phase within the collagen network endures the stress of collagen fibrils, whereas the collagen is predominantly responsible for the material deformation response.[9,10] In this regard, mineral content of collagen is crucial to determine the mechanical characteristics and functionality of bone.[2]

Among synthetic methods for the mineralization of collagen it is worth of mentioning perfusion-based mineralization,[11] direct blending of collagen and mineral crystals,[12,13] the mineral co-precipitation during collagen fibrillogenesis,[14,15] immersion of collagen scaffolds into simulated body fluid (SBF),[16] the self-assembly and mineralization by vapour diffusion,[17] and the direct nucleation of apatite onto collagen fibrils.[18,19]

Lanthanides ions, such as terbium ions ($Tb^{3+}$), exhibit exceptional photoluminescence properties in the visible and near-infrared region, and present important biological applications: labelling in diagnosis and control of disease development.[20] $Tb^{3+}$ substitutes $Ca^{2+}$ in the apatitic structure and endows it with luminescence, photocatalytic properties, and bactericidal activity. At low $Tb^{3+}$ doping, $Tb^{3+}$-substituted nanoapatites retained the physicochemical and biological benefits of the apatite, although is harmful for the organism at high concentrations.[20,21] The implantation of $Tb^{3+}$-substituted nanoapatites in bone defects has allowed to determine the distribution of these nanocrystals and to track their degradation during new bone formation by using laser scanning confocal microscopy (two photons) in combination with other techniques.[22,23]

In this work, we propose the simultaneous self-assembly and mineralization of type I collagen molecules by a base-acid neutralization method to yield collagen-apatite fibrils with

varying extent of mineralization. Two variants of the method have been explored: base-acid titration, a solution of $Ca(OH)_2$ was added dropwise to a stirred solution containing type I collagen dispersed in $H_3PO_4$; and direct mixing, the $Ca(OH)_2$ solution was added by fast dripping onto the acidic solution. Additionally, the influence of $Tb^{3+}$ in the mineralization process has been tested to obtain luminescent Col/Ap nanocomposites with potentiality to act as an implantable diagnostic tool in bone tissue engineering. In a further step, we studied the cytocompatibility of the samples and their ability to induce osteogenic differentiation of human mesenchymal stem cells (hMSCs).

## 2. Results

### 2.1. Crystallographic and spectroscopic features

#### *2.1.1. X-ray diffraction patterns*

The X-ray diffraction (XRD) patterns of samples prepared by the base-acid titration variant at reagent concentrations C1, C2, C3 (where C2=0.5 C1 and C3=0.1C1, see Table 1) and Col/CaP ratios 50:50, 70:30 and 90:10 (wt%) are shown in **Figure 1** (a-c). When using the higher concentration of reagents (C1), both the patterns of the control CaP and of the Col/CaP samples are composed of a mixture of apatite (JCPDS 09-432), brushite (DCPD, JCPDS #11-293), and calcium carbonate (calcite phase, JCPDS #05-0586).

Apatite displays its main distinguishing reflections, for example the peaks at 2θ = 25.87° corresponding to the crystallographic (002) plane, the wide peak corresponding to the triplet at 31.77°, 32.19° and 32.90° (planes (211), (112) and (300)) respectively, the reflections at 39.82° and 46.71° (planes (310) and (222)) and other minor peaks in the 2θ range from 47°-65°.[24] In the Col/CaP 90:10 sample, the reflections of apatite are negligible. The bulging of the baseline indicates the presence of the amorphous phase of calcium phosphate, ACP. It is worth to mention that the wide peak involving the triplet in the 2θ range from 31°-33° indicates the

nanocrystalline character of the apatite. Similar results are found when the concentration of reagents decreases to C2. However, when using the concentration C3 the diffractogram of the control sample merely shows the presence of apatite without any additional crystalline phase. The Col/CaP 50:50 is composed of apatite, brushite and calcite, and both the Col/CaP 70:30 and Col/CaP 90:10, only of apatite and calcite, with a decreased proportion of calcite, as noted by the decrease of the relative peak intensity of the reflection at 2θ 29.4°.

**Table 1** summarizes the precipitated solid phases, with major phases highlighted in bold. The pH titration curves (see Supporting Information **Figure S1**) reveal the more abrupt changes of the pH for experiments CaP and Col/CaP 50:50 while the softer ones for Col/CaP 90:10. These zones of pH contain the equivalence point, where the precipitation reaction reached the chemical balance. However, as the titration curves were extended beyond this point, the final pHs were high enough, enabling the precipitation of $CaCO_3$ (calcite).

Figure 1d shows the XRD patterns of samples prepared by direct mixing of solutions of concentration C2, in absence and presence of type-I collagen, at Col/CaP ratios (wt%) 50:50, 70:30 and 90:10. In these experiments, the XRD patterns correspond to the apatite phase except in the case Col/CaP 90:10, which yielded calcite with a minor proportion of apatite. The presence of the wide peak within the 2θ range from 31°-33° reflects the nanocrystalline character of the particles. The effect of $Tb^{3+}$ in the direct mixing experiments is shown in Figure 1e. As it is observed, in both cases the precipitates are formed of apatite and, in them, the calcite phase has been suppressed or strongly reduced.

### *2.1.2. FTIR features of control samples and mineralized collagen fibrils*

The spectrum of type I collagen control (**Figure 2**) revealed the typical signals of amide A (3290 $cm^{-1}$; N–H stretching), amide B (~3075 $cm^{-1}$, weak second component of stretching N-H or stretching vibration of intramolecularly hydrogen bonded NH groups,[25] and amides I

(~1652 $cm^{-1}$, stretching C=O ), II (1541 $cm^{-1}$, stretching C-N), and III (~1236 $cm^{-1}$, C–N stretching coupled with N–H bending),[26] which are associated with the triple helical conformation of the type I collagen fibrils. The FTIR spectrum of this sample also exhibits bands at ~2920 $cm^{-1}$ assigned to the $CH_2$ asymmetrical stretching, and at 2852 $cm^{-1}$ ($CH_2$ symmetrical stretching). Absorption bands at 1449, 1398, 1339, 1276, 1236, 1205 $cm^{-1}$ can be attributed to the $\delta(CH_2)$, $\delta(CH_3)$, $\nu$(C-N) and $\delta$(N-H) absorptions of collagen; additional absorptions at 1064 and 1035 $cm^{-1}$(shoulder) arise from $\nu$(C-O-C) and $\nu$(C-O) of the carbohydrate moieties. [27]

Also important is the characterization of the CaP control sample (so-called CaP control) prepared by base-acid titration. The main distinguishing FTIR absorption bands of this sample were found in the wavenumber range between 3600 $cm^{-1}$ and 2600 $cm^{-1}$ as well as in the region from 1800 to 400 $cm^{-1}$ (Figure 2a). The first one is dominated by the OH stretching of adsorbed water with a small band at around 3533 $cm^{-1}$ and 3474 $cm^{-1}$ that are assigned to the OH stretching of the apatite component. The 400-1800 $cm^{-1}$ region shows typical spectral features of calcium phosphate compounds. The main band at 1000-1100 $cm^{-1}$ corresponds to the asymmetric stretching mode of $PO_4^{3-}$ groups ($\nu_3PO_4$). The peak at ~984 $cm^{-1}$ is ascribed to the symmetric stretching ($\nu_1PO_4$) while less intense bands at ~601 and 571 $cm^{-1}$ are due to the bending mode of $PO_4^{3-}$ groups ($\nu_4PO_4$). The band at ~518 $cm^{-1}$ in the $\nu_4PO_4$ domain can be assigned to $HPO_4^{2-}$ ions,[28] in this case of the brushite phase ($CaHPO_4.H_2O$). The presence of carbonate ($CO_3^{2-}$) bands is attested by vibrational signatures due to the $\nu_3CO_3$ mode, and can be attributed to the presence of calcium carbonate (calcite). The carbonate ($CO_3^{2-}$) bands also appear when carbonated apatite is present in the sample, the vibrational signatures due to the $\nu_3CO_3$ mode appear around 1421 $cm^{-1}$ and 1462 $cm^{-1}$, and the $\nu_2CO_3$ mode with a bulging peak around 871 $cm^{-1}$, which may be attributed to B-type substitution, with $CO_3^{2-}$ replacing $PO_4^{3-}$ groups in the apatite structure.[28]

The FTIR spectra of samples Col/CaP 50:50 and Col/CaP 70:30 show some of typical absorption bands of collagen such as the amide A (~3270 $cm^{-1}$), amide B (~3100 $cm^{-1}$) and less intense amides I at around 1646 and amide III at 1220 $cm^{-1}$, respectively. The amides A and B are partially overlapped with the $H_2O$ band between 3600 $cm^{-1}$ and 2600 $cm^{-1}$. The presence of apatitic -OH stretching is observed at around 3530 and 3470 $cm^{-1}$. The wavelength range from 400-1800 $cm^{-1}$ is dominated by the asymmetric stretching mode of $PO_4^{3-}$ groups ($\nu_3PO_4$) of apatite at 1000-1100 $cm^{-1}$, the symmetric stretching ($\nu_1PO_4$) at 985$cm^{-1}$, the bands at ~601 and 568 $cm^{-1}$ which are due to the bending mode of $PO_4^{3-}$ groups ($\nu_4PO_4$) and the band at ~520 $cm^{-1}$ which is assigned to non-apatitic (surface) $HPO_4^{2-}$ ions. In addition to the phosphate bands the carbonate ($CO_3^{2-}$) bands arise at around 1410-1470 $cm^{-1}$ ($\nu_3CO_3$ mode) and the $\nu_2CO_3$ mode around 871 $cm^{-1}$, which can be attributed to B-type substitution, with $CO_3$ replacing $PO_4^{3-}$ groups in the apatite structure.[28] The same bands arise in the FTIR spectra of sample Col/CaP 90:10 but in this case the amide II band is more intense and the $\nu_4PO_4$ region is poorly defined. It is worth to highlight that in this sample the proportion of CaP in the sample is lower than in the two other Col/CaP composites.

In the presence of $Tb^{3+}$ the $\nu_3PO_4$ appears at 1022 $cm^{-1}$ and the $\nu_4PO_4$ vibration is attested by peaks at 599 and 561 $cm^{-1}$ characteristic of the apatitic phase. The $CO_3^{2-}$ bands also appear being the band at 873 $cm^{-1}$ characteristic of B-type substitution. In these spectra the amides A and B of the $Tb^{3+}$-Col/CaP samples are overlapped with the $H_2O$ band between 3600 $cm^{-1}$ and 2600 $cm^{-1}$. It must be remembered that apatite was the precipitated phase in these samples with a negligible proportion of calcite. Concerning bands of collagen, the amides A and B of the $Tb^{3+}$-Col/CaP samples are found overlapped with the $H_2O$ band between 3600 $cm^{-1}$ and 2600 $cm^{-1}$.

Additional characterizations by Raman spectroscopy of assembled type I collagen and Col/CaP samples obtained by titration using concentration C2 are shown in **Figure S2**.

**2.2. Morphological features of mineralized fibrils**

The products of assembly and mineralization were mineralized collagen fibrils and a CaP precipitate attached to the fibrils. **Figure 3** shows TEM images and SAED patterns (as insets) of mineralized fibrils prepared by titration at concentrations C1 and C3, respectively: collagen control (Figure 3a,f), Col/CaP 90:10 (Figure 3b,g), Col/CaP 70:30 (Figure 3c,h) and Col/CaP 50:50 (Figure 3d,i), as well as of the additional CaP precipitated outside the fibrils (CaP control, Figure 3e,j). In average, as the extent of mineralization increased, the nanocrystalline coating onto the collagen fibrils increased. The main difference between C1, C2 and C3 lie in the decreased amount of CaP precipitated outside the fibrils when decreasing the reagent concentration. The SAED pattern recorded in selected fibril areas shows two distinguishable but poorly highlighted rings that correspond to the crystallographic (002) and (112) planes of the apatite (Figure 3b,c,d,i insets).[30,31] It indicates fibril gaps have been mineralized by poorly crystalline apatite incipiently formed in these samples, having particle sizes around 100-120 nm; however, in Col/CaP 70:30 (Figure 3h, inset), the diffuse rings of the SAED pattern indicate ACP. This phase is also found in Col/CaP 90:10 (Figure 3g) with particle size around 60-70 nm. Hence, significant differences have been achieved regarding the nature of the mineral and the extent of mineralization of the fibers, at least from a qualitative view, from low mineralized fibrils (Col/CaP 90:10) to fully mineralized fibrils (Col/CaP 50:50).

Moreover, the SAED analysis of the extra CaP precipitate accompanying the Col/CaP 50:50 sample (Figure 3e) revealed two phases: apatite and dicalcium phosphate dehydrate (DCPD, $CaHPO_4 \cdot 2H_2O$, brushite),[31,32] whose SAED pattern show a recognizable ring attributed to its (-141) plane. DCPD crystals display laminar morphology with length of 1200-1500 nm, while apatites show needle-like shapes with lengths around 90-110 nm. Figure 3j, instead, shows that apatite with lengths 50-60 nm was the only extra phase outside the mineralized fibrils. Analysing collagen controls and Col/CaP 90:10 fibrils in Figure 3, it can be seen the typical

banding pattern of 67 nm periodicity in both cases, showing the right self-assembly of the collagen fibrils obtained by this method.

The mineralized fibrils Col/CaP obtained with concentrations C2 by the direct mixing variant were inspected by VPSEM. **Figure 4** shows visual differences between the mineralization extent from Col/CaP 90:10 to 50:50 (Figure 4b-d) using Col as control (Figure 4a). However, the nature of the neutralization product presents certain differences, according to the XRD patterns of Figure 1d. Once again, ACP coated the 90:10 sample, while apatite coated 70:30 and 50:50.

The TEM micrographs of the mineralized fibrils and bulk precipitate of Col/CaP 70:30 sample show nanoparticles of similar size and same morphology, which are identified by SAED (Figure 4f, inset) as apatite. Their lengths were 120-160 nm. Similar findings are observed in sample Tb-doped Col/CaP 70:30, with apatite lengths of 80-120 nm. The ratio (Tb+Ca)/P was 2.14±0.09 in the mineralized fibrils, and 1.81 ± 0.04 in the apatite outside the fibrils (Ca,P and Tb analyzed by EDS), indicating successful incorporation of the lanthanide both into the apatite phase coating the collagen and outside the fibrils.[33]

### 2.3.Luminescence properties of $Tb^{3+}$-doped collagen-apatite fibrils

Some lanthanides, i.e. $Eu^{3+}$ and $Tb^{3+}$, form highly fluorescent chelates with many different organic ligands. The sensitized fluorescence results from the ligand absorbing light, the energy of which is then transferred to the chelated metal ion. In fact, $Tb^{3+}$ emits the energy as narrow-banded, line-type fluorescence with a long Stokes shift (over 250 nm) and an exceptionally long fluorescence decay time (up to 1 ms).[34] Because of the long fluorescence decay time (over 10 times longer than the average background fluorescence) of these doped materials, a delay time ($t_d$) and a gate time ($t_g$) can be used during the measuring, remarkably reducing the background

fluorescence. The luminescence properties of solid $Tb^{3+}$-doped Col/CaP samples are depicted in **Figure 5**, which shows the uncorrected excitation and emission spectra.

For the $Tb^{3+}$-doped Col/CaP only the excitation wavelength at 225 nm was observed (Figure 5a). The broad bands between 200 and 300 nm, centered at 225 nm, correspond to charge transfer (called charge transfer band, CTB), which occurs by electron delocalization from the filled 2p shell of $O^{2-}$ to the partially filled 4f shell of $Tb^{3+}$. Also, this band can partially be attributed to the charge transfer transition $X^{5+}$–$O^{2-}$.[35,36] The emission spectra show several narrow bands. For $Tb^{3+}$-doped material they are centered at 490, 545, 586 and 620 nm which correspond to the $Tb^{3+}$ $^5D_4 \rightarrow {}^7F_6$, $^5D_4 \rightarrow {}^7F_5$, $^5D_4 \rightarrow {}^7F_4$ and $^5D_4 \rightarrow {}^7F_3$ transitions, respectively.[37] The emission wavelength corresponding to the hypersensitive transition without inversion center ($^5D_4 \rightarrow {}^7F_5$, 545 nm for $Tb^{3+}$) produces the highest relative luminescence intensity (R.L.I.). Therefore, the optimum excitation and emission wavelengths were 225 and 548 nm respectively.

Figure 5b also shows that the control sample, free of $Tb^{3+}$, do not show any luminescence emission when exciting at 225 nm, thus it is possible to deduce that the luminescent properties of these materials are only due to the incorporation of $Tb^{3+}$. In addition, the Col/CaP ratio affects the luminescence properties of the composites; this effect is more pronounced in $Tb^{3+}$-doped Col/CaP 90:10, indicating that a clear decrease for apatite provides an increase on the luminescence intensity.

Concerning the luminescence lifetime (τ), **Figure S3** shows a decrease of the R.L.I. versus time for $Tb^{3+}$-doped materials. The decay profile of the $Tb^{3+}$-doped samples were not possible to fit properly with a single exponential component,[38] and, therefore, a biexponential decay ($RLI = A_1 \cdot e^{-t/\tau 1} + A_2 \cdot e^{-t/\tau 2} + C$) was used. It can be attributed to inhomogeneous distribution of the $Tb^{3+}$ in the hosting material.[38] In this case, $Tb^{3+}$ can dope both components of the composite, the apatite and the collagen. On the other hand, the phenomenon can be also attributed to non-radiative recombination that involves the enhanced multiphoton decay of localized exciton state (lower luminescence lifetime), and the radiative decay of these localized exciton states (higher

luminescence lifetime).[39,40] The decay curve of the control Col/CaP sample (free of $Tb^{3+}$) was flat indicating that no sensitized luminescence was recorded. Therefore, it is not represented in Figure S3. For $Tb^{3+}$-doped Col/CaP samples the luminescence lifetime almost doubled that of $Tb^{3+}$-doped CaP. However, the lifetime of the sample $Tb^{3+}$-doped Col/CaP 90:10 increased to 1850 μs. This spectacular increase of lifetime can be due to the incorporation of $Tb^{3+}$ in the structure of CaP and on the collagen.

Finally, **Figure 6a** shows the luminescence emission of $Tb^{3+}$-doped Col/CaP 90:10 fibrils as well as of the undoped material (left) and the corresponding bulk CaP samples (right), under sunlight (up), and under UV illumination. The luminescent emission of the doped 90:10 samples is very intense and it can be seen by naked eye. Under white light, all materials are white. Under UV illumination bulk $Tb^{3+}$-CaP shows green color. However, in the case of Col/CaP 90:10 the nanocomposite presents a blue color due to the blue fluorescence emission of collagen (emission at 490 nm). In the case of $Tb^{3+}$-Col/CaP is turquoise. The turquoise is a mixed colour due to fluorescence emissions of both materials. **Figure 6b** shows optical microscopy and two-photon confocal fluorescence microscopy images of Col, Col/CaP 70:30 and $Tb^{3+}$-Col/CaP 70:30. It is clearly observed the green luminescence emission of the $Tb^{3+}$-doped composite using an excitation wavelength of 458 nm, which is not harmful to bone tissue, and can allow tracking the alterations of the composite when implanted in a bone defect.

## 2.4. Biological tests of mineralized collagen samples

### *2.4.1. Cytotoxicity and viability assays on human mesenchymal stem cells (hMSCs)*

The effect of Col/CaP 50:50, 70:30 and 90:10 samples obtained by titration, direct mixing, and direct mixing $Tb^{3+}$-doped, at reagent concentration C2, on the viability of hMSCs were tested after 72h of exposition (**Figure 7a**).

The hMSCs viability cultured in presence of titration samples shows a maintenance >80% with respect to MSCs control (100%) at all tested concentrations, anyhow higher than 70% which is still associated to a good cell viability and represent the cut-off indicated by ISO 10993–5:2009.[41] hMSCs cultured in presence of direct mixing samples both undoped and $Tb^{3+}$-doped showed cell viabilities > 90%, and even higher than 100% in samples Col/CaP 70:30, which represent a significant increase of cell proliferation compared to control.

Additionally, to evaluate the feasibility of mineralized fibrils as an adequate support for cell survival, the viability of MSCs on fibrils pellets was evaluated. Different mineralization grades, Col/CaP 90:10, 70:30, 50:50 (wt%) at reagent concentration C2 prepared by titration, were visualized with the live/dead staining using confocal microscopy after 7 days of MSCs pellet formation. Confocal images (**Figure 7b**) demonstrated hMSCs growing on all mineralized fibrils, thus showing good cell survival with few dead cells after 7 days in culture.

### *2.4.2. Evaluation of the osteogenic differentiation potential of Col/CaP samples*

hMSCs were cultured in monolayer and induced to differentiate toward an osteogenic linage by the addition of osteogenic differentiation medium (ODM) or by the addition of titration, direct mixing and $Tb^{3+}$-doped Col/CaP samples. Alizarin Red staining was used to determine calcium mineral salt deposit formation in hMSCs cultures, ability developed in the early stages of differentiation into osteoblasts.[42] hMSCs control culture (hMSCs control) does not exhibit any mineral deposit, while hMSCs maintained with ODM and hMSCs cultured in presence of CaP control prepared by titration exhibited large clusters with bright red appearance indicating the presence of extracellular mineral deposit (**Figure 8a**).

Osteogenic differentiation of hMSCs in presence of titration Col/CaP samples observed after 10 days in culture shows mineral deposition to be present mainly on cells around the collagen fibrils, and in more amount in the higher mineralized fibrils (Col/CaP 70:30 and 50:50).

As expected, normal cell growth was found in the collagen control without mineral phase. Compared to titration samples, mineral deposits increased in presence of direct mixture samples, indicating enhanced osteogenic differentiation of hMSCs. The osteogenic differentiation was even more pronounced when using the $Tb^{3+}$-doped samples, demonstrating that the higher apatite density of the fibrils, especially Col/CaP 50:50, the higher the mineral deposit. Quantification of stained areas of **figure 8a** confirmed these trends, although no statistical differences were found in the case of Col/CaP 90:10 samples (**Figure 8b**).

## 3. Discussion

The aim of this work was the preparation of mineralized type I collagen-apatite fibrils with varying mineralization extent and doped with luminescent bactericidal $Tb^{3+}$to endow them of luminescent properties, of great interest in bone tissue regeneration to track alterations of the fibrils when implanted in a bone defect.

Precipitation experiments were carried out by a base-acid neutralization method. It was found that the titration variant of this technique yielded, on average, mineralized fibrils with ACP or apatite plus a precipitate composed of CaP polymorphs and calcite. The reason for this crystallographic issue was the poor kinetic control of the precipitation process, due to the slow increase of pH (as shown in the titration curves in Figure S1). Consequently, besides the more stable CaP phase, the apatite, other metastable phases had enough time to nucleate and grow in the crystallization medium. These metastable phases were ACP and brushite, whose stability was influenced by the pH of the medium. As example, brushite is very stable at pHs below 6.5;[43,44] thus a slow increase of pH favoured its appearance in the medium. Additionally, the pH titration curves were completed beyond the pH of the equivalence point, where the precipitation reaction reached the chemical balance, therefore the excess of $Ca^{2+}$ in contact with the dissolved $CO_2$ in the suspension was responsible for the formation of $CaCO_3$ (calcite). These extra CaP phases were not found in the Col/CaP fibrils analysed by SAED, but outside the

fibrils. The titration variant was very useful to mineralize the fibrils with varying mineralization extent (Figure 3), simply by varying the initial reagent concentrations (Col/CaP) from ratios 90:10 to 50:50 (wt%).

The direct mixing variant (fast crystallization) allowed us a better kinetic control of the crystallization and to better solve the crystallographic issue, obtaining the nanocrystalline apatite phase as mineral component, not only of the Col/CaP fibril but also as additional phase precipitated outside the fibrils. The exception was the less mineralized sample (90:10) where ACP was once again the phase coating the collagen nanofibers. In addition, these low mineralized samples were accompanied of calcite. Generally in these experiments, though solutions of $Ca(OH)_2$ and $H_3PO_4$ were prepared to get Ca:P atomic ratios 5:3, the final pHs were basic due to excess of $OH^-$ and calcite was not found or strongly reduced due to the lack of free $Ca^{2+}$ after ACP or apatite precipitation. Altering the mineralization extent of the collagen, and arranging the mineralized collagen fibrils in multilayers mimicking the different layers of native osteochondral structures, has been a strategy to fabricate scaffolds for bone replacement.[45] The method used in our work to alter the mineralization extent of the fibrils can be very useful regarding this type of applications.

Interesting results were obtained when adding luminescent lanthanide $Tb^{3+}$ ions to the reaction mixture: even the 90:10 samples were composed of apatite coating the fibrils and as additional phase precipitated outside the fibrils. The results of decay time of the R.L.I as well as of luminescence lifetime of the $Tb^{3+}$-doped materials suggest that $Tb^{3+}$ ions are integrated into both components of the Col/CaP fibril, the collagen and the apatite. The finding could be attributed to the lower ionic radius of $Tb^{3+}$ (0.92 Å) with respect to that of $Ca^{2+}$ (0.99 Å) [20,46] which allows $Tb^{3+}$ to $Ca^{2+}$ substitution in the apatite crystal lattice. The different R.L.I. and lifetimes obtained for the different $Tb^{3+}$-Col/CaP fibrils also suggest that luminescence properties of the composites could be tailored for a given biological imaging application. In fact, they could be used in fluorescence microscopy without labelling with an additional

fluorescent dye, for instance the $Tb^{3+}$-doped Col/CaP materials displaying green fluorescence when inspected under two-photons fluorescence confocal microscopy could be useful as such without labelling with FITC (fluorescein, green fluorescence).

Biocompatibility of mineralized fibrils is essential for their uses in clinical applications. Biocompatibility of Col/CaP fibrils on hMSCs was assessed by AlamarBlue® assays. Cell viability assays showed that all the mineralized nanocomposites prepared were non cytotoxic and biocompatible in accordance with previous results, where CaP deposits were used to improve the surface properties of artificial implants on human fetal osteoblast and human gingival fibroblasts.[47] The results of hMSCs cytotoxicity assays, at 72 hours of culture, showed that titration samples exhibited a cell viability of more than 80%, whereas proliferation of hMSCs on direct mixing Col/CaP samples was even better. This finding was attributed to the presence of only nanoapatite accompanying the mineralized fibrils. $Tb^{3+}$-doped nanocomposites also showed a good cytocompatibility, with cell viabilities higher than 95%. This was because terbium increases the rate of adherence of MSCs by upregulating the expression of adhesion molecules.[48] Nanoapatite works as a reservoir of $Ca^{2+}$ and $PO_4^{3-}$ ions necessary for a variety of metabolic functions, because of a continuous resorption and formation of nanodimensional apatite by osteoclasts and osteoblasts, respectively.[2,49,50] The presence of nanocrystalline apatite without any additional amorphous and crystalline phase into or over self-assembled collagen fibrils has exhibited before a more favourable cell proliferation and viability, to optimize biological functionality.[51,52] Moreover, the live/dead viability/cytotoxicity assay showed good cell survival after 7 days of MSCs pellet culture in mineralized fibrils. These results confirmed the cell viability and indicated that mineralized fibrils can provide optimal growth conditions.

Then, we explored the possibility that Col/CaP samples can induce osteogenic differentiation without the presence of osteogenic supplements, such as dexamethasone, β-glycerol phosphate, and ascorbic acid. The set of samples obtained by titration demonstrated

that mineralized collagen fibrils promoted the osteogenic differentiation, inducing a calcium salt deposition in hMSCs.[42] However, mineralized fibrils obtained by direct mixing variant showed better results, likely because of the homogeneity in composition of the samples regarding the CaP phase. These samples were basically composed of nanocrystalline apatite, whose presence promotes osteogenesis at a higher level than other CaP.[52–54] Concerning $Tb^{3+}$-doped samples we appreciated even greater osteogenic activity. It was reported that $Tb^{3+}$ participates in the metabolic pathways of osteogenic differentiation through the activation of the transforming growth factor β/bone morphogenetic protein, osteogenic genes upregulation; and by the inhibition of peroxisome-proliferator-activated receptor γ2, adipogenic genes downregulation.[48] Future studies aim to evaluate the osteogenic differentiation potential of apatite mineralized 3D collagen scaffolds fabricated with the proposed method by assessing the expression of osteogenic markers such as alkaline phosphatase, osteopontin and osteocalcin.

All together, these data show the capability of the proposed method to yield biomimetic Col/CaP with varying mineralization extent, tailored luminescence, high cytocompatibility and high ability to induce the osteogenic differentiation of hMSCs. The latter was enhanced when samples were prepared by the direct mixing variant, and especially with the $Tb^{3+}$-doped composites, and open new perspectives for *in vivo* applications, namely in the fields of bone tissue engineering, regenerative medicine and *in vivo* imaging.

## 4. Conclusion

The experiments of self-assembly and mineralization of type I collagen by base-acid titration yielded, mostly, mineralized fibrils with nanocrystalline apatite plus a powder composed of apatite, brushite, and calcite, while those performed by direct mixing led, mostly, to fibrils mineralized with nanocrystalline apatite plus apatite powder, due to better kinetic control of the crystallization process. Both methods allowed the preparation of Col/CaP

nanocomposites with varying mineralization extent, mimicking the different layers of native osteochondral structures.

In the presence of $Tb^{3+}$ we obtained luminescent $Tb^{3+}$-doped Col/Ap nanocomposites with long luminescent lifetimes and high relative luminescence intensities, where $Tb^{3+}$ doped the apatite phase and also was integrated onto the collagen. The prepared nanocomposites did not present cytotoxicity when they were in contact with hMSCs. Furthermore, though all they promoted the osteogenic differentiation of hMSCs, the effect was more pronounced when in contact with mineralized Col/Ap fibrils prepared by direct mixing, and more notably when using the $Tb^{3+}$-doped Col/Ap fibrils.

## 5. Experimental Section/Methods

*Materials*. Type I collagen extracted from equine tendon was provided from OPOCRIN Spa (Corlo di Formigine, MO, Italy). Calcium hydroxide ($Ca(OH)_2$, ≥ 96.0 pure) was acquired to Fluka. Orthophosphoric acid ($H_3PO_4$, ACS reagent, ≥ 85% in $H_2O$) and Terbium (III) chloride anhydrous ($TbCl_3$, powder, 99.9% trace metals basis), were purchased to Sigma-Aldrich. All solutions were prepared with ultrapure water (0.22 μS, 25 °C, Milli-Q, Millipore).

*Synthesis and characterization*. Experiments of simultaneous self-assembly and mineralization were carried out by neutralization method. Disassembled fibrils were prepared by dispersing the raw collagen in stirring $H_3PO_4$ solution for one day. We used two variants of the neutralization method: 1) base-acid titration in which a $Ca(OH)_2$ solution was added dropwise onto a stirring solution containing type I collagen dispersed in $H_3PO_4$ until reaching a chemical balance,[55] and 2) direct mixing, in which the base was added into the acid solution by fast dripping. Suspensions were left in magnetic stirring for 2 hours at 25°C and then washed either with abundant ultrapure water in 50 μm mesh sieves or by ultracentrifugation at 9000 rpm for 15 minutes. Finally, samples were freeze-dried overnight at -50°C under vacuum (3 mbar). Mineralized fibrils were collected with tweezers under an optical microscope. They contained

aggregated CaP powder difficult to remove. Experiments were designed to produce nanocomposites with Col/CaP ratios 50:50, 70:30 and 90:10 wt% using three reagent concentrations [C1= $Ca(OH)_2$ (0.368g, 0.5 M) + $H_3PO_4$ (147,8 µL, 0.3 M) in ultrapure water (10 mL); C2=1/2 C1; C3=1/10 C1]. In the direct mixing variant, we tested the concentration C2 and the influence of $Tb^{3+}$ using $Tb^{3+}/Ca^{2+}$ molar ratios of 1:9.

The pH of solutions and suspensions was measured by a Crison 5208 pH probe connected to a Crison GLP21 pH-meter (Crison Instruments, S.A., Spain). Mineralized fibrils were characterized by X-ray diffraction (XRD) between 4° to 70° 2θ in transmission mode, with a Bruker D8 Advance Vario diffractometer (Bruker GmbH, Karlsruhe, Germany), using CuKα1 radiation (1.5406 Å). FTIR spectra were recorded in transmittance mode within the wavenumber range from 4000 $cm^{-1}$ to 400 $cm^{-1}$ using a JASCO 6200 spectrometer provided of an attenuated total reflectance (ATR) accessory of diamond crystal (JASCO, Tokyo, Japan). A complementary spectroscopic characterization of some selected samples was performed by a JASCO NRS-5100 Micro-Raman spectrometer ($\lambda_{exc}$=785 nm). Transmission electron microscopy (TEM) and selected area electron diffractions (SAED) were performed with a Carl Zeiss Libra 120 TEM microscope (Carl Zeiss, Jena, Germany) operating at 80 kV. The samples were dispersed ultrasonically in ultrapure water, and then a Formvar coated copper microgrid was soaked in a drop of this preparation prior to observation. Scanning electron microscopy observations were performed with a Variable Pressure SUPRA40VP (Carl Zeiss, Jena, Germany) scanning electron microscope (VPSEM), provided of a large X-Max 50 mm area detector for energy dispersive X-ray spectroscopy (EDS) microanalysis. Few mineralized fibrils were selected from each experiment and deposited on conventional supports, which were carbon-sputtered before the observation.

*Luminescence spectroscopy.* The luminescence properties (excitation and emission spectra and lifetime) of $Tb^{3+}$-doped solid samples were recorded using a Cary Eclipse Varian Fluorescence Spectrophotometer (Varian Australia, Mulgrave, Australia). A front surface accessory was used

to obtain the luminescence spectra, the luminescence lifetime and the relative luminescence intensities of the samples. The instrumental parameters for characterizing the solid particles in powder were: $\lambda_{exc}$= 225 nm, $\lambda_{em}$= 545 nm, slit-widths$_{exc/em}$= 10/10 nm, delay time ($t_d$)= 0.120 µs, gate time ($t_g$)= 5 ms and detector voltage= 450 V for $Tb^{3+}$ -doped materials. Fluorescence confocal microscopy images (two-photon) of $Tb^{3+}$-doped material were taken with a High Speed Spectral Confocal Microscope and Multiphoton Leica TCS-SP5 II Instrument. The instrumental parameters used were the following: $\lambda_{exc}$= 458 nm (20%), $\lambda_{em}$= 465-530 nm, photomultiplier hybrid bright mode 230%, and pinhole = 150µm using a bidirectional sequential objective 512x512.

*hMSCs isolation and culture from adipose tissue:* hMSCs used in this study were isolated from human adipose tissue and characterized as previously shown.[56] All samples of adipose tissue were collected with informed consent and Institutional Review Board approval (ethic permission number: 02/022010 Hospital Virgen de la Victoria, Málaga, Spain). Cells were cultured with high-glucose Dulbecco's modified Eagle's medium (DMEM; Sigma-Aldrich, St Louis, MO, USA) supplemented with 10% fetal bovine serum (FBS; Sigma-Aldrich), 100 U/mL penicillin and 100 mg/mL streptomycin (Invitrogen Inc., Grand Island, NY, USA) at 37°C in a humidified atmosphere containing 5% $CO_2$. The medium was regularly changed every 3 days. At 80% of confluence, cells were subcultured. Cells were used between passages 4 and 6 for all the experiments.

*Cytotoxicity tests*: The effect of Col/CaP 50:50, 70:30 and 90:10 (wt%) samples at reagent concentration C2 on cells was assessed using AlamarBlue® assay (Bio-Rad Laboratories, Inc., Hercules, CA, USA). Alamar Blue is a redox indicator, i.e. it responds to reduction or oxidation of the surrounding medium. Col/CaP samples were sterilized under UV light. Control CaP powders were dispersed in DMEN and filtered through a pore size of 0,22 µm. Cells were seeded onto 48-well plates with a density of $10\times10^3$ cells/well. The culture medium was changed 24 h after and then cells were kept in contact with the different Col/CaP samples at

concentrations 10, 100 and 500 μg/ml for 72h. Thereafter, they were incubated with 10 μL of Alamar Blue solution per each 100 μL of culture medium and incubated for 3h. After 3h of incubation at 37°C, fluorescence intensity was quantified at $\lambda_{exc}$ 530 nm and $\lambda_{em}$ of 590 nm in a Synergy® HT multi-detection microplate reader (BioTek Instruments, Inc., Winooski, VT, USA). Collagens and CaP powders were used as controls.

*Viability tests*: Cell viability in cell pellets with mineralized fibrils was determined using Live/Dead™ Viability/Cytotoxicity Kit (Invitrogen Inc., Grand Island, NY, USA). For pellet formation, 1 mg of collagen, Col/CaP 90:10, 70:30, 50:50 (wt%) samples at reagent concentration C2 prepared by titration and by direct mixture was mixed with 250000 MSCs, in 15 mL conical tube with 2 mL of DMEM medium. The mixture was spun down (1200 rpm, 7 minutes), and all mineralized collagen samples/MSCs mix was cultured overnight at 37°C and 5% $CO_2$ to form a cell pellet. Then, pellets were incubated for 1 week, medium was changed every three days and the tubes were gently shaken to avoid the adherence of the pellet to the plastic walls. MSCs viability after 7 days of culture were evaluated by the live/dead staining, using 1 μM calcein AM and 2 μM ethidium homodimer-3 in DMEM supplemented with 10% (v/v) FBS to stain dead cells in red and live cells in green. After staining, pellets were washed with phosphate-buffered saline (PBS), fixed in 4% paraformaldehyde. Samples were observed in a confocal microscopy Nikon Eclipse Ti-E A1 (Nikon Instruments Europe B.V., Amsterdam Netherlands).

*Osteogenic differentiation assays:* MSCs plated at $10\times10^3$ cells/well were seeded onto 48-well plates. Once the cells were confluent, the culture medium was replaced with DMEM (Sigma-Aldrich) containing 10% FBS (Sigma-Aldrich) and 1% penicillin/streptomycin, and supplemented with 100μg/ml of collagen, CaP, Col/CaP 50:50, Col/CaP 70:30 or Col/CaP 90:10. Positive controls of osteogenic differentiation were cultured with osteogenic differentiation medium (ODM) DMEM (Sigma-Aldrich) containing 10% FBS (Sigma-Aldrich), and 1% penicillin/streptomycin, L-ascorbate acid (50 μg/mL), β -glycerophosphate (10

mmol/L) and dexamethasone (10 nmol/L). Medium was replaced every 3 days. After 10 days of osteogenic differentiation culture, differentiated cells were stained with 40 mM Alizarin Red S solution (Sigma–Aldrich), pH 4.2 at room temperature for 10 min. Samples were then rinsed 3 times in distilled water on an orbital shaker. The stained matrixes were microphotographed by inverted light microscope. Quantification of calcified area was performed using NIH ImageJ.

Supporting Information
Supporting Information is available from the Wiley Online Library or from the author.

**Acknowledgements**
This work was funded by the Ministerio de Ciencia, Innovación y Universidades, co-funded by FEDER (projects PGC2018-102047-B-I00 and RTC-2016-5451-1) and by Fundación Mutua Madrileña (project FMM-AP17196-2019). We also acknowledge technicians of VPSEM, TEM and confocal microscopy of CIC of University of Granada for their valuable support.

**Conflicts of interest**
The authors declare no conflicts of interest

Received: ((will be filled in by the editorial staff))
Revised: ((will be filled in by the editorial staff))
Published online: ((will be filled in by the editorial staff))

**References**

[1] S. Dorozhkin, *J. Funct. Biomater.* **2015**, 6, 708.

[2] S. Weiner, H.D. Wagner, *Annu. Rev. Mater. Sci.* **1998**, 28, 271.

[3] M.D. Shoulders, R.T. Raines, *Annu. Rev. Biochem.* **2009**, 78, 929.

[4] J.P.R.. Orgel, A. Miller, T.C. Irving, R.F. Fischetti, A.P. Hammersley, T.J. Wess, *Structure.* **2001**, 9, 1061.

[5] H.-N. Su, L.-Y. Ran, Z.-H. Chen, Q.-L. Qin, M. Shi, X.-Y. Song, X.-L. Chen, Y.-Z. Zhang, B.-B. Xie, *Nanoscale*. **2014**, 6, 8134.

[6] S. Varma, J.P.R.O. Orgel, J.D. Schieber, *Biophys. J.* **2016**, 111, 50.

[7] J. Gómez-Morales, M. Iafisco, J.M. Delgado-López, S. Sarda, C. Drouet, *Prog. Cryst. Growth Charact. Mater.* **2013**, 59, 1.

[8] K. Ishikawa, *Materials (Basel).* **2010**, 3, 1138.

[9] A.K. Nair, A. Gautieri, S.-W. Chang, M.J. Buehler, *Nat. Commun.* **2013**, 59, 1724.

[10] R. Murugan, S. Ramakrishna, *Compos. Sci. Technol.* **2005**, 65, 2385.

[11] B. Antebi, X. Cheng, J.N. Harris, L.B. Gower, X.-D. Chen, J. Ling, *Tissue Eng. Part C Methods.* **2013**, 19, 487.

[12] G. Tomoaia, R.-D. Pasca, *Clujul Med*. **2015**, 88, 15.

[13] D. Zhang, X. Wu, J. Chen, K. Lin, *Bioact. Mater.* **2018**, 3, 129.

[14] J.-H. Bradt, M. Mertig, A. Teresiak, W. Pompe, Chem. Mater. **1999**, 11, 2694.

[15] M. Kikuchi, S. Itoh, S. Ichinose, K. Shinomiya, J. Tanaka, *Biomaterials*. **2001**, 22, 1705.

[16] F.-Z. Cui, Y. Li, J. Ge, *Mater. Sci. Eng. R Reports.* **2007**, 57, 1.

[17] G.B. Ramírez-Rodríguez, M. Iafisco, A. Tampieri, J. Gómez-Morales, J.M. Delgado-López, *J. Mater. Sci. Mater. Med.* **2014**, 25, 2305.

[18] A. Tampieri, M. Sandri, E. Landi, D. Pressato, S. Francioli, R. Quarto, I. Martin, *Biomaterials*. **2008,** 29, 3539.

[19] A. Tampieri, G. Celotti, E. Landi, M. Sandri, N. Roveri, G. Falini, *J. Biomed. Mater. Res. Part A.* **2003**, 67, 618.

[20] T. Tite, A.-C. Popa, L.M. Balescu, I.M. Bogdan, I. Pasuk, J.M.F. Ferreira, G.E. Stan, *Materials (Basel).* **2018**, 11, 2081.

[21] L. Li, Y. K. Liu, J. Tao, M. Zhang, H. Pan, X. Xu, R. Tang, *J. Phys. Chem. C.* **2008**, 112, 12219.

[22] X. Li, Q. Zou, H. Chen, W. Li, *Sci. Adv.* **2019**, 5, 2375.

[23] Y. Il Park, K.T. Lee, Y.D. Suh, T. Hyeon, *Chem. Soc. Rev.* **2015**, 44, 1302.

[24] F.J. Martínez-Casado, M. Iafisco, J.M. Delgado-López, C. Martínez-Benito, C. Ruiz-Pérez, D. Colangelo, F. Oltolina, M. Prat, J. Gómez-Morales, *Cryst. Growth Des.* **2016**, 16, 145.

[25] A. Barth, *Biochim. Biophys. Acta - Bioenerg.* **2007**, 1767, 1073.

[26] T. Riaz, R. Zeeshan, F. Zarif, K. Ilyas, N. Muhammad, S.Z. Safi, A. Rahim, S.A.A. Rizvi, I.U. Rehman, *Appl. Spectrosc. Rev.* **2018**, 53, 703.

[27] K. Belbachir, R. Noreen, G. Gouspillou, C. Petibois, *Anal. Bioanal. Chem.* **2009**, 395, 829.

[28] N. Vandecandelaere, C. Rey, C. Drouet, *J. Mater. Sci. Mater. Med.* **2012**, 23, 2593.

[29] T.T. Nguyen, C. Gobinet, J. Feru, S. Pasco, M. Manfait, O. Piot, *J. Spectrosc*. **2012**, 27, 421.

[30] J.-K. Kim, Y.-E. Kwon, S.-G. Lee, J.-M. Jeong, J.-G. Kim, Y.-J. Kim, *Mater. Charact.* **2017**, 135, 1.

[31] R. Downs, M. Hall-Wallace, *American Mineralogist*, **2003**, 88(1), 247.

[32] S.F. Mansour, S.I. El-dek, M.A. Ahmed, S.M. Abd-Elwahab, M.K. Ahmed, *Appl. Nanosci.* **2016**, 6, 991.

[33] K. Byrappa, T. Ohachi, Crystal Growth Technology, Elsevier, **2003**.

[34] I. Hemmilä, S. Dakubu, V.-M. Mukkala, H. Siitari, T. Lövgren, *Anal. Biochem.* **1984**, 137, 335.

[35] K.P.F. Siqueira, P.P. Lima, R.A.S. Ferreira, L.D. Carlos, E.M. Bittar, F.M. Matinaga, R. Paniago, K. Krambrock, R.L. Moreira, A. Dias, *J. Phys. Chem. C.* **2015**, 119, 17825.

[36] K.P.F. Siqueira, P.P. Lima, R.A.S. Ferreira, L.D. Carlos, E.M. Bittar, E. Granado, J.C. González, A. Abelenda, R.L. Moreira, A. Dias, *Chem. Mater.* **2014**, 26, 6351.

[37] F.S. Richardson, *Chem. Rev.* **1982**, 82, 541.

[38] S. Dutta, S. Som, S. Sharma, *RSC Adv.* **2015**, 5, 7380.

[39] R. Klann, O. Brandt, H. Yang, H.T. Grahn, K.H. Ploog, Recombination Dynamics of Near-Bandedge Emission in Cubic GaN, in: O. Svelto, S. De Silvestri, G. Denardo (Eds.), Ultrafast Process. Spectrosc., Springer US, Boston, MA, 1996: pp. 259–263. https://doi.org/10.1007/978-1-4615-5897-2_59.

[40] T. Gokus, L. Cognet, J.G. Duque, M. Pasquali, A. Hartschuh, B. Lounis, *J. Phys. Chem. C.* **2010**, 114, 14025.

[41] ISO 10993-5:2009 - Biological evaluation of medical devices - Part 5: Tests for in vitro cytotoxicity; Available online: https://www.iso.org/standard/36406.html (accessed on Nov 5, 2018)., in: n.d.

[42] G.L. Lin, K.D. Hankenson, *J. Cell. Biochem.* **2011**, 112, 3491.

[43] M. Iafisco, M. Marchetti, J. Gómez Morales, M.A. Hernández-Hernández, J.M. García Ruiz, N. Roveri, *Cryst. Growth Des.* **2009**, 9, 4912.

[44] L. Wang, G.H. Nancollas, *Chem. Rev.* **2008**, 108, 4628.

[45] E. Beniash, *Wiley Interdiscip. Rev. Nanomed. Nanobiotechnol.* **2011**, 3, 47.

[46] I.A. Neacsu, A.E. Stoica, B.S. Vasile, E. Andronescu, *Nanomaterials.* **2019**, 9, 239.

[47] S. V Dorozhkin, *Mater. Sci. Eng. C.* **2015**, 55, 272.

[48] D.-D. Liu, K. Ge, Y. Jin, J. Sun, S.-X. Wang, M.-S. Yang, J.-C. Zhang, *J. Biol. Inorg. Chem.* **2014**, 19, 879.

[49] S. V Dorozhkin, *J. Mater. Sci.* **2007**, 42, 1061.

[50] S. V Dorozhkin, *Materials (Basel).* **2009**, 2, 399.

[51] S. V Dorozhkin, *Materials (Basel).* **2009**, 2, 1975.

[52] S.-J. Xu, Z.-Y. Qiu, J.-J. Wu, X.-D. Kong, X.-S. Weng, F.-Z. Cui, X.-M. Wang, *Tissue Eng. Part A.* **2015**, 22, 170.

[53] Y. Li, T. Jiang, L. Zheng, J. Zhao, *Mater. Sci. Eng. C.* **2017**, 80, 296.

[54] A. Sujana, J.R. Venugopal, B. Velmurugan, A. Góra, M. Salla, S. Ramakrishna, *J. Tissue Eng. Regen. Med.* **2017**, 11, 1853.

[55] J.R. Harris, A. Reiber, *Micron.* **2007**, 38, 513.

[56] E. López Ruiz, G. Jiménez González, W. Kwiatkowski, E. Montañez, F. Arrebola, E. Carrillo, S. Choe, J.A. Marchal, M. Perán, *Eur. Cells Mater.* **2018**, 35, 209.

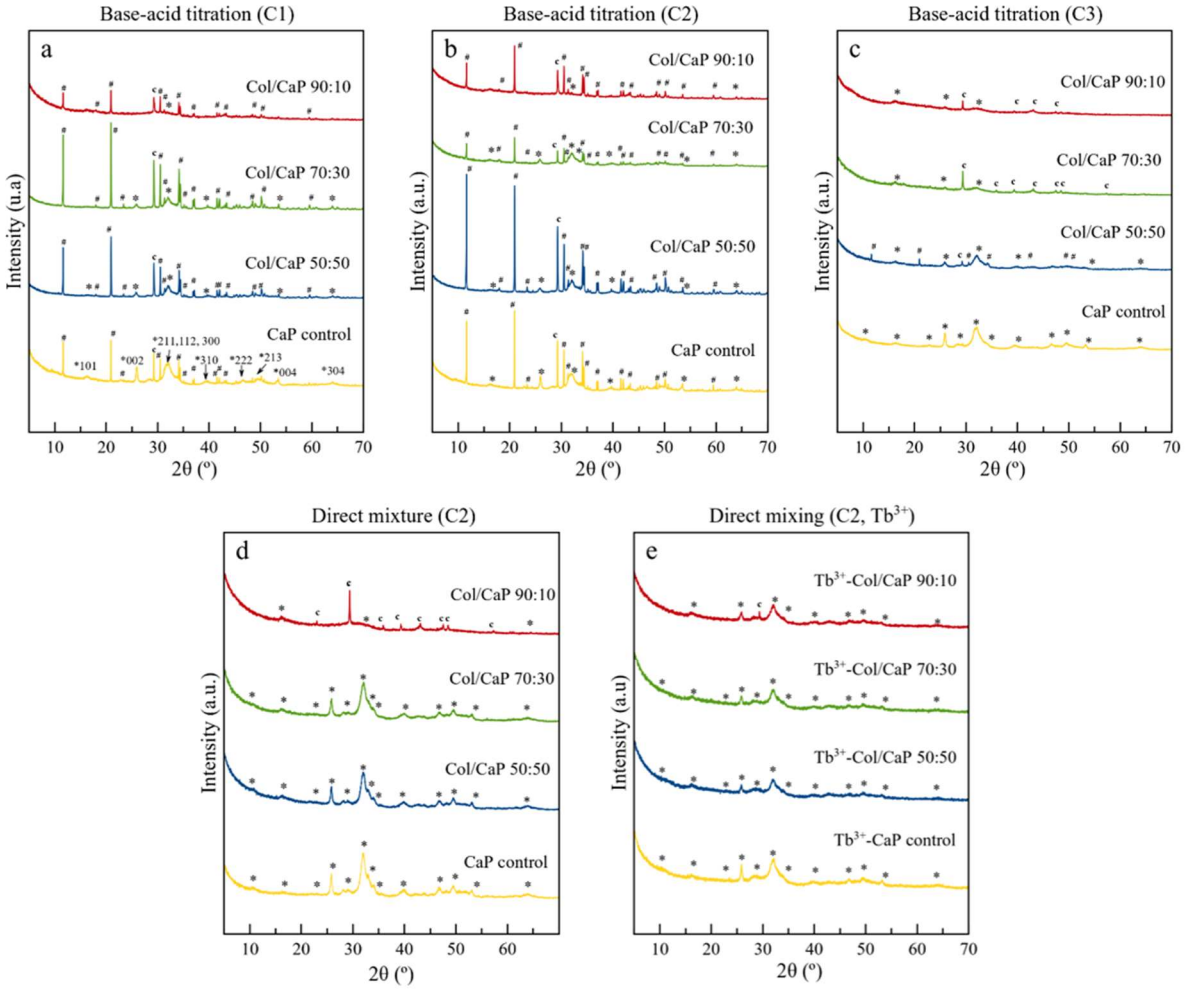


**Figure 1.** X-ray diffraction patterns of CaP control and Col/CaP 50:50, 70:30 and 90:10 samples: (a-c) prepared by base-acid titration at reagent concentrations C1, C2 and C3, (d) prepared by direct mixing at reagent concentration C2, and (e) prepared by direct mixing at C2 in presence of $Tb^{3+}$. # brushite; * apatite; c calcite.

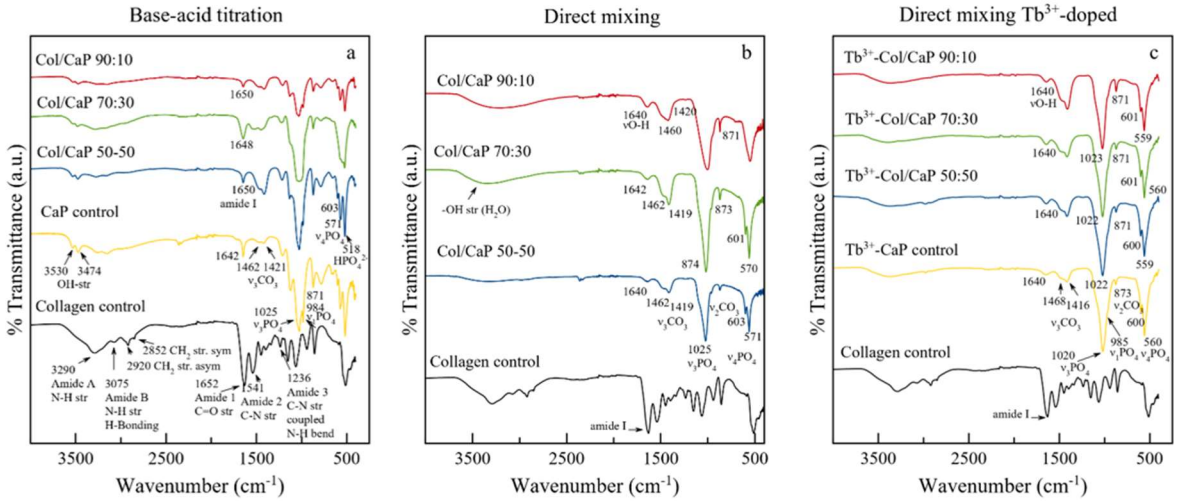


**Figure 2.** FTIR spectra of samples Collagen control, CaP control, and Col/CaP 50:50, 70:30, 90:10 prepared with a concentration of reagents C2: (a) by titration, (b) by direct mixing, and (c) by direct mixing in presence of $Tb^{3+}$.

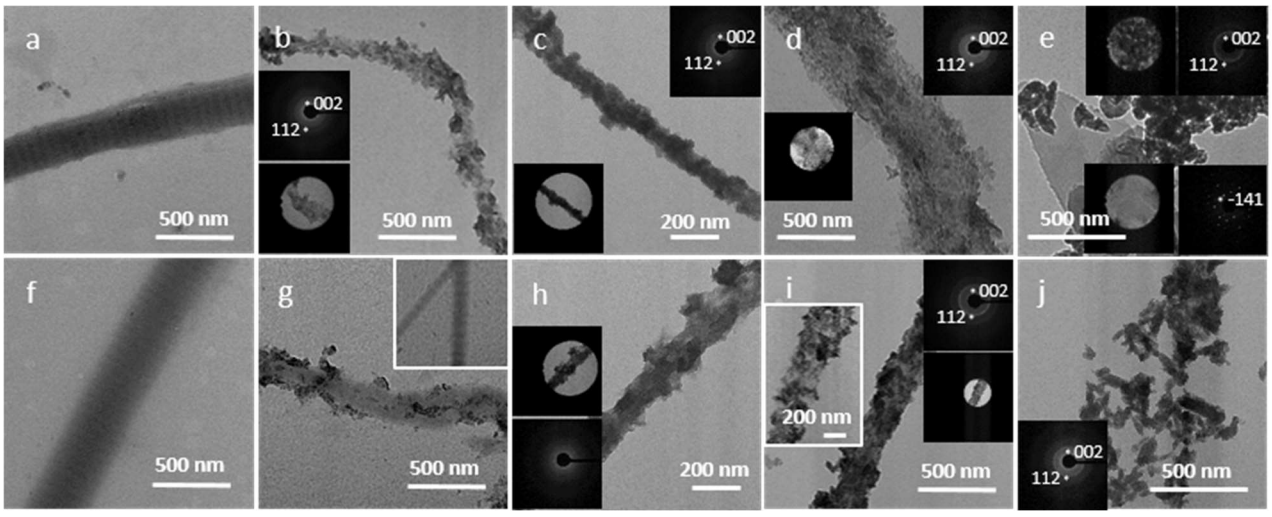


**Figure 3.** TEM micrographs of mineralized type-1 collagen fibrils by base-acid titration method using reagent concentrations C1 (first file) and C2 (second file): (a, f) self-assembled type 1-collagen control samples; (b, g) Col/CaP 90:10; (c, h) Col/CaP 70:30; (d, i) Col/CaP 50:50; (e, j) precipitated solid phases out of the fibrils. Insets in figures b, c, d, e, h, j, and i are the SAED patterns recorded in the fibrils samples.

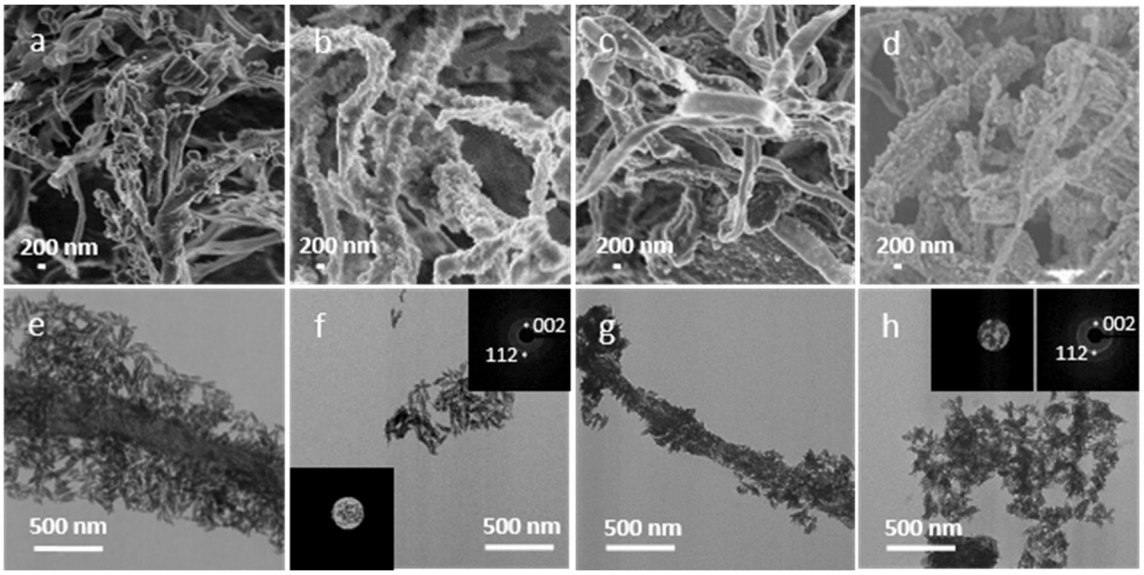


**Figure 4.** (a-d) VPSEM micrographs of mineralized fibrils prepared by the direct mixing variant: (a) Col; (b) Col/CaP 90:10; (c) Col/CaP 70:30; (d) Col/CaP 50:50; TEM images of Col/CaP 70:30 samples (e), the bulk precipitate (f), Col/Tb-CaP (g), and the bulk precipitate (h). Insets in micrographs f and h show the SAED patterns.

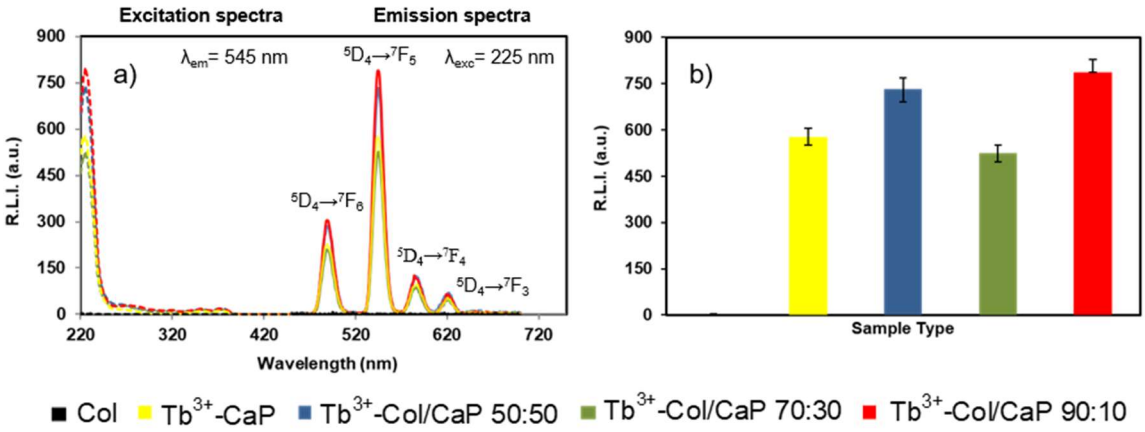


**Figure 5.** a) Excitation (dashed lines) and emission (solid lines) spectra of $Tb^{3+}$-doped Col/CaP with different apatite content. Slit-widths$_{exc/em}$= 10/10 nm, detector voltage = 450v, $t_d$= 120 µs and $t_g$= 5 ms. b) Relative luminescence intensity (R.L.I.) of different $Tb^{3+}$-doped Col/CaP and control samples.

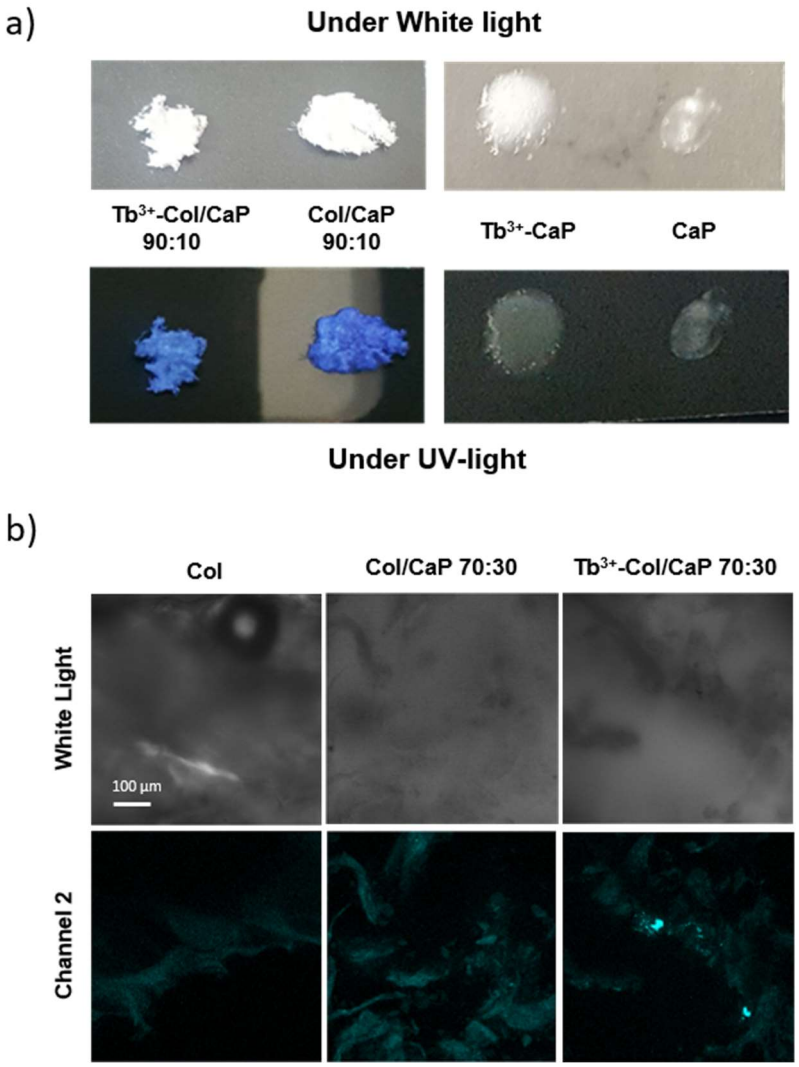


**Figure 6**. a) Pictures of $Tb^{3+}$-Col/CaP 90:10 and Col/CaP 90:10 (left), and $Tb^{3+}$-CaP and CaP (right) under sunlight (up) and 324 nm UV–lamp illumination (down). b) White light and two-photon laser confocal microscopy images of Col (a), Col/CaP 70:30 (b) and $Tb^{3+}$-Col/CaP 70:30 (c) using excitation wavelength of 458 nm. Scale bar equal for all images.

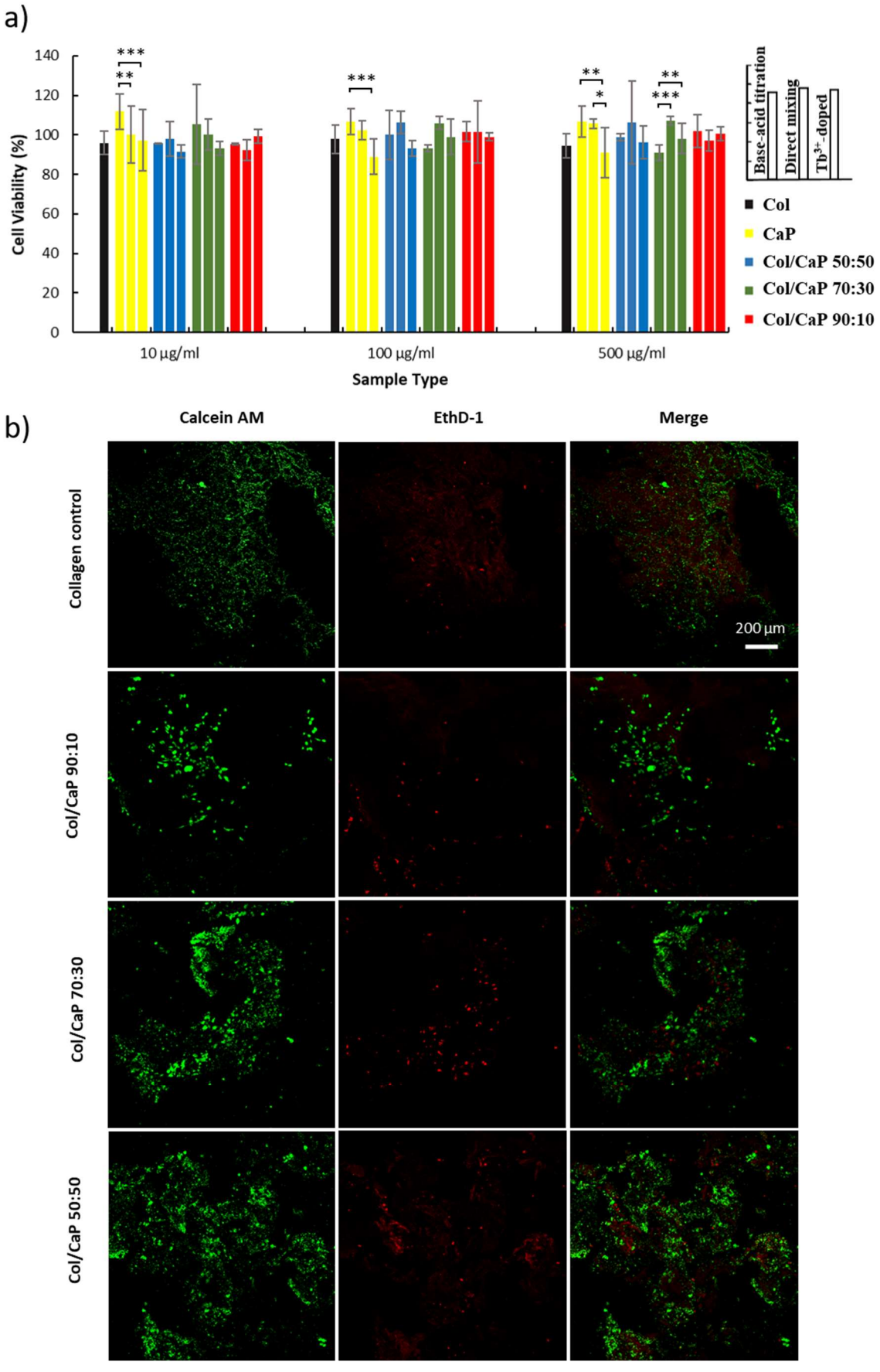


**Figure 7.** Cytocompatibility of hMSCs on mineralized fibrils. a) hMSCs viability after 72 hours of incubation with AlamarBlue® in presence of Col, CaP, Col/CaP 50:50, Col/CaP 70:30 and

Col/CaP 90:10, prepared at C2. In each triplet, the first bar corresponds to the titration sample, the second bar to the direct mixture sample, and the third one to $Tb^{3+}$-doped. All values are expressed as percentage versus the positive control (hMSCs in a culture media). Significant differences, * $p<0.05$, ** $p<0.01$ and *** $p<0.001$. b) Representative confocal images of hMSCs cultured on self-assembled collagen fibrils used as control and Col/CaP 90:10, 70:30 and 50:50 (wt%) samples at reagent concentration C2 obtained by titration at day 7. Live/dead® assay was used, live cells were stained green with calcein AM while dead cells were stained with ethidium homodimer red. Scale bars: 200 µm.

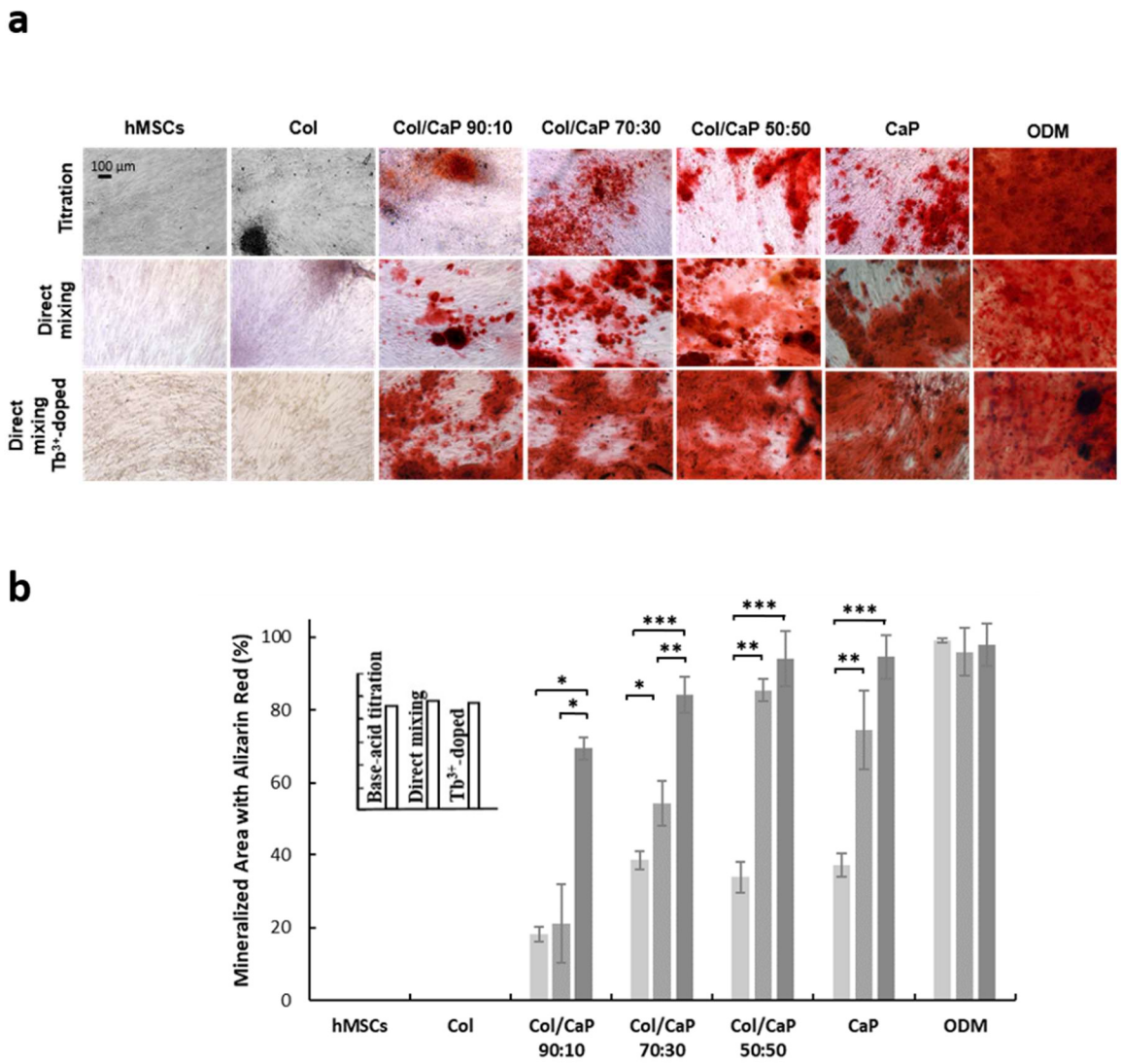


**Figure 8.** Osteogenic differentiation assays of hMSCs in cultures treated with 100 µl/ml of Col, Col/CaP, CaP control and ODM (Osteogenic Differentitation Media) after 10 days (titration samples) or 13 days (direct mixing and $Tb^{3+}$-doped samples). a) Examination of calcium deposits based on Alizarin Red S staining. Scale bar of 100 µm is the same for all images. b) Quantification of alizarin red S stained area given by NIH ImageJ. Statistical significance of mineralization between titration, direct mixing and $Tb^{3+}$-doped samples at each apatite density of the fibrils using Student's t-test, * $p<0.05$, ** $p<0.01$ and *** $p<0.001$.

**Table 1.** Experimental conditions of type-1 collagen assembly and mineralization including the methodology, reagent concentration, pH of reagents solutions, final pH, and the precipitated solid phases identified by X-ray diffraction.

| Sample identification | Reagent concentrations and method | pHs (Acid Initial; Base Initial; Final) | Precipitated solids phases |
|---|---|---|---|
| Col/CaP 50:50 | C1, T | 1.23; 12.96; 12.96 | **Apatite, DCPD**, **$CaCO_3$ (calcite)** |
| Col/CaP 50:50 | C2, T | 1.29; 12.79; 12.77 | **Apatite, DCPD**, **$CaCO_3$ (calcite)** |
| Col/CaP 50:50 | C3, T | 1.85; 13.04; 12.55 | **Apatite**, DCPD, $CaCO_3$ (calcite) |
| Col/CaP 70:30 | C1, T | 1.39; 12.93; 12.93 | **Apatite, DCPD, $CaCO_3$ (calcite)** |
| Col/CaP 70:30 | C2, T | 1.60; 12.94; 12.87 | **Apatite, DCPD, and $CaCO_3$ (calcite)** |
| Col/CaP 70:30 | C3, T | 2.21; 12.46; 8.46 | ACP/Apatite, **$CaCO_3$ (calcite)** |
| Col/CaP 90:10 | C1, T | 1.86; 13.01; 12.15 | ACP/Apatite, **DCPD, $CaCO_3$ (calcite)** |
| Col/CaP 90:10 | C2, T | 2.05; 12.53; 10.89 | ACP/Apatite**, DCPD, $CaCO_3$ (calcite)** |
| Col/CaP 90:10 | C3, T | 2.56; 12.17; 7.4 | ACP/Apatite, $CaCO_3$ (calcite) |
| Col/CaP 50:50 | C2, MD | 1.43; 12.57; 11.75 | **Apatite** |
| Col/CaP 70:30 | C2, MD | 1.71; 12.56; 11.47 | **Apatite** |
| Col/CaP 90:10 | C2, MD | 2.08; 12.53; 10.26 | ACP/Apatite, **$CaCO_3$ (calcite)** |
| $Tb^{3+}$-Col/CaP 50:50 | C2, MD | 1.18; 12.45; 9.5 | **Apatite** |
| $Tb^{3+}$-Col/CaP 70:30 | C2, MD | 1.44; 12.52; 9,92 | **Apatite** |
| $Tb^{3+}$-Col/CaP 90:10 | C2, MD | 1.83; 12.57; 11.36 | **Apatite**, $CaCO_3$ (calcite) |
| CaP (blank) | C1, T | 1.23; 12.96; 12.96 | **Apatite, DCPD**, **$CaCO_3$ (calcite)** |
| CaP (blank) | C2, T | 1.29; 12.79; 12.77 | **Apatite, DCPD**, **$CaCO_3$ (calcite)** |
| CaP (blank) | C3, T | 1.85; 13.04; 12.55 | **Apatite** |
| CaP (blank) | C2, DM | 1.43; 12.57; 11.75 | **Apatite** |
| $Tb^{3+}$-CaP (blank) | C2, DM | 1.52; 12.07; 9.61 | **Apatite** |
| Col (blank) | C1*, DM | 1.36; 13.32; 7.20 | **Self-assembled collagen fibrils** |

C1=0.5 M $Ca(OH)_2$ + 0,3 M $H_3PO_4$; C2=1/2 C1; C3=1/10 C1; C1*= 0,9 M NaOH+0,3 M $H_3PO_4$; T= base-acid titration; DM= direct mixing; ACP= amorphous calcium phosphate; DCPD= brushite; major phases are highlighted in bold.